Early Afterslip Deformation Captured by Sub-Daily Kinematic GPS following the 2010 Mw 7.8 Mentawai Earthquake

Anandiko Savieros Sujanto[1], Putra Maulida[1], Mokhamad Nurcahyadi[1], Ira Mutiara Anjasmara[1], Agnis Triahadini[2]*

[1]Department of Geomatics Engineering, Institut Teknologi Sepuluh Nopember, Surabaya, Indonesia
[2]Department of Geophysics Engineering, Institut Teknologi Sepuluh Nopember, Surabaya, Indonesia

*Corresponding author: putra@its.ac.id

Abstract. On 25 October 2010, an Mw 7.8 earthquake occurred west of the Mentawai Islands, releasing energy from a shallow offshore fault and generating complex ground deformation patterns. Although surface deformation has been monitored for over a decade, the precise geometry of the slipping zone remains unresolved. This study investigates the event using sub-daily kinematic GPS observations from the Sumatra GPS Array (SuGAr) to analyze coseismic and early postseismic deformation following the rupture. The resulting displacement field reveals limited horizontal motion of approximately 20–25 cm and vertical subsidence of about 4–6 cm near the islands, suggesting that most slip was concentrated offshore toward the trench. In the subsequent days, the GPS time series displays a gradual decay in motion, which can be modeled with a logarithmic function and characteristic timescales of roughly five days. This transient response is interpreted as an early afterslip evolving downdip of the main rupture area. These findings underscore the heterogeneous nature of the plate interface, where seismic and aseismic processes occur concurrently over short timescales. Future work will estimate early afterslip using a time-dependent inversion model to further characterize the rupturing zone and clarify the transition between seismic and aseismic deformation.

1 Introduction

1.1 Background

The subduction zone where the Indo-Australian plate dives beneath the Sunda block is recognized globally as a high-risk tectonic boundary, historically producing massive megathrust earthquakes [1]. The Mentawai segment is particularly notable within this system for its potential to generate "tsunami earthquakes" rare events that cause tsunamis far larger than their seismic magnitude would suggest [2]. This threat became reality in 2010 when a shallow section of the megathrust ruptured west of the Pagai Islands (Mw 7.8) [3]. Unlike typical powerful earthquakes, this event was marked by slow rupture propagation and weak high-frequency radiation, yet it unleashed a destructive tsunami with run-ups reaching 16 meters [3]. Such ruptures within the shallow accretionary prism challenge the prevailing assumption that the updip end of the seismogenic zone is predominantly aseismic or resistant to slip, underscoring the need for improved understanding of the frictional properties of the shallow plate boundary [4]. Following the mainshock's rapid release of accumulated strain, the resulting stress change typically induces significant aseismic movement, known as afterslip, which can persist for months or years [5]. This postseismic period is critical for elucidating fault zone properties, as it often accounts for a substantial portion of total displacement and can increase stress on adjacent fault segments [6]. Previous geodetic studies of the Sumatra-Andaman system have demonstrated that afterslip is a principal postseismic process. For instance, afterslip following the 2007 magnitude 8.4 Bengkulu earthquake increased stress on the adjacent Mentawai segment, potentially accelerating the 2010 event [7]. While the long-term decay of afterslip has been extensively studied using daily GPS data, the evolution of this process during the initial minutes to hours after rupture the early postseismic phase remains poorly understood [8].

The main obstacle to characterizing this early phase is the limited temporal resolution of standard geodetic techniques. Conventional processing typically utilizes daily static GPS solutions, which average coordinates over 24-

hour windows to maximize precision [9]. Although this approach is effective for tracking long-term tectonic rates, the temporal averaging acts as a low-pass filter, effectively masking the rapid transient motions that occur right after an earthquake [10]. Recent studies using high-rate, sub-daily kinematic GPS have shown that substantial displacement occurs within this initial window. In standard daily processing, this early motion is often incorrectly lumped into the coseismic estimate [8]. For example, analyses of the 2010 Maule and 2015 Illapel earthquakes revealed that ignoring this early phase can lead to an underestimation of the postseismic slip budget and a misunderstanding of the fault's frictional heterogeneity [8]. Accurately resolving these displacements is crucial for assessing the full energy budget of large earthquakes and characterizing the transition from seismic to aseismic slip [8].

This observational gap is particularly relevant for the 2010 Mentawai event, which ruptured a region previously considered to be weakly coupled [11]. To overcome these resolution limitations, this study employs sub-daily kinematic GPS observations from the Sumatra GPS Array (SuGAr) to reconstruct high-frequency displacement waveforms associated with the 2010 earthquake. By utilizing a kinematic processing approach instead of daily solutions, the analysis aims to pinpoint the precise onset of afterslip and distinguish it from the true coseismic offset. Furthermore, the Principal Component Analysis-based Inversion Method (PCAIM) is applied to model the spatiotemporal evolution of slip [12]. This methodology facilitates the detection of rapid logarithmic decay signals that are often aliased in conventional processing, thereby providing new constraints on the frictional properties of the shallow megathrust and enhancing the understanding of the slip budget associated with tsunami earthquakes [13].

2 Materials and methods

2.1 Geodetic data

Continuous GPS observations were obtained from the Sumatra GPS Array (SuGAr), a network jointly operated by the Earth Observatory of Singapore (EOS) and BRIN [3], [7]. This array offers ideal near-field coverage of the Mentawai segment. We focused our analysis on 16 stations situated on Sipora, North Pagai, and South Pagai Islands (including BSAT, PRKB, SLBU), as these locations lie directly above the rupture's downdip limit. By utilizing high-rate sampling (15 seconds), we were able to capture sub-daily crustal motions that are typically smoothed out in standard 24-hour geodetic solutions [8].

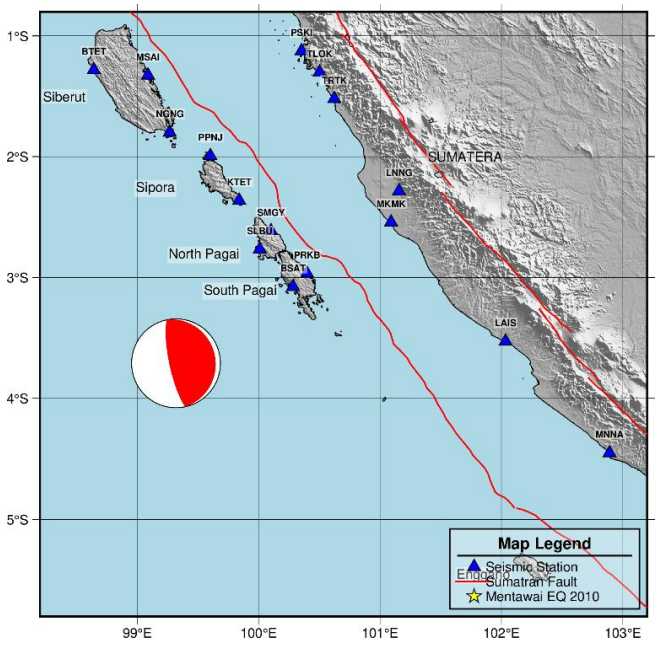

Fig. 1 *Study Area*

2.2 Kinematic PPP processing

To retrieve instantaneous station positions, we processed the raw GPS observables using the GipsyX software package from NASA's Jet Propulsion Laboratory (JPL) [14]. Instead of using network-based double-difference methods, we applied the Precise Point Positioning (PPP) technique [15], which enables the autonomous and precise determination of coordinates for individual stations.

Data were processed using the GipsyX software [14] employing the Precise Point Positioning (PPP) strategy [15]. We utilized JPL's final orbits and clock products, applied single-receiver ambiguity resolution, and aligned coordinates to ITRF2014 with VMF1 tropospheric corrections.

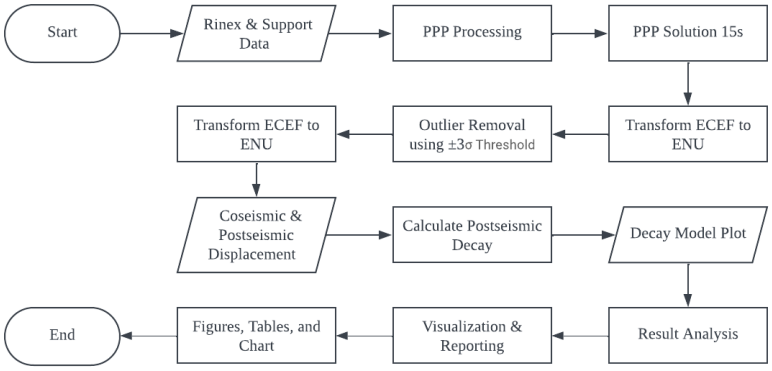

Fig. 2 *Research Workflow*

2.3 Filtering and signal extraction

Kinematic time series inherently contain high-frequency noise and outliers caused by multipath effects and receiver instability. To extract the tectonic signal, we implemented a post-processing filtering strategy. A sidereal filter was applied to remove repeating multipath patterns based on the satellite constellation's repeat cycle. Additionally, spatial filtering was used to mitigate common-mode errors (CME) that affect the regional network. To ensure data integrity, outliers exceeding three times the standard deviation (3σ) were iteratively removed. This cleaning process effectively eliminates non-geophysical artifacts, yielding a clean displacement waveform suitable for inversion and ensuring that the modeled decay represents true ground deformation rather than observational noise [8].

2.4 Displacement and Decay Visualization

The cleaned kinematic time series reveals three distinct components of deformation: long-term secular tectonic motion, an abrupt coseismic jump, and transient postseismic relaxation. To separate these signals, we first calculated the displacement from the preseismic baseline to the coseismic step, and then tracked the position change from the coseismic moment through the minutes, hours, and days of early postseismic deformation. The temporal evolution of this postseismic motion was modeled using the following equations:

$$u(t) = c + a \ln\left(1 + \frac{t}{\log \tau}\right) \quad (1)$$

$$u(t) = c + a\left(1 - e^{-\frac{t}{\tau exp}}\right) \quad (2)$$

Here, u(t)denotes the position at time t (meters), c is the coseismic offset (m), a is the amplitude of the transient decay, t is the time elapsed since the mainshock (days), log τ represents the characteristic timescale for logarithmic decay, and τ_{exp} is the exponential decay constant. The logarithmic term describes the early afterslip mechanism, defined by its decay amplitude and characteristic time τ [5]. In this analysis, we explicitly differentiate rapid near-field afterslip from long-term viscoelastic relaxation, as previous studies have demonstrated that logarithmic decay offers a better fit for early postseismic deformation in the days immediately following an earthquake [13].

3 Result and Discussion

3.1 Kinematic Time Series and Decay Analysis

To characterize the deformation associated with the 2010 Mentawai earthquake, we first analyzed the 15-second kinematic position estimates derived from the SuGAr network. Unlike standard daily static solutions, which provide only a single coordinate averaged over a 24-hour period, our sub-daily kinematic time series reveal the continuous evolution of crustal motion from the precise moment of rupture (t=0) through the early postseismic phase. The displacement time series for the North and East components at important near-field stations, including SLBU, BSAT, KTET, and LNNG, display a clear tectonic signal, as seen in Fig. 3. Despite the high-frequency scatter inherent in sub-daily solutions attributable to unmodeled short-term tropospheric variability and multipath effects the tectonic trend remains unmistakable and clearly distinguishable from observational noise.

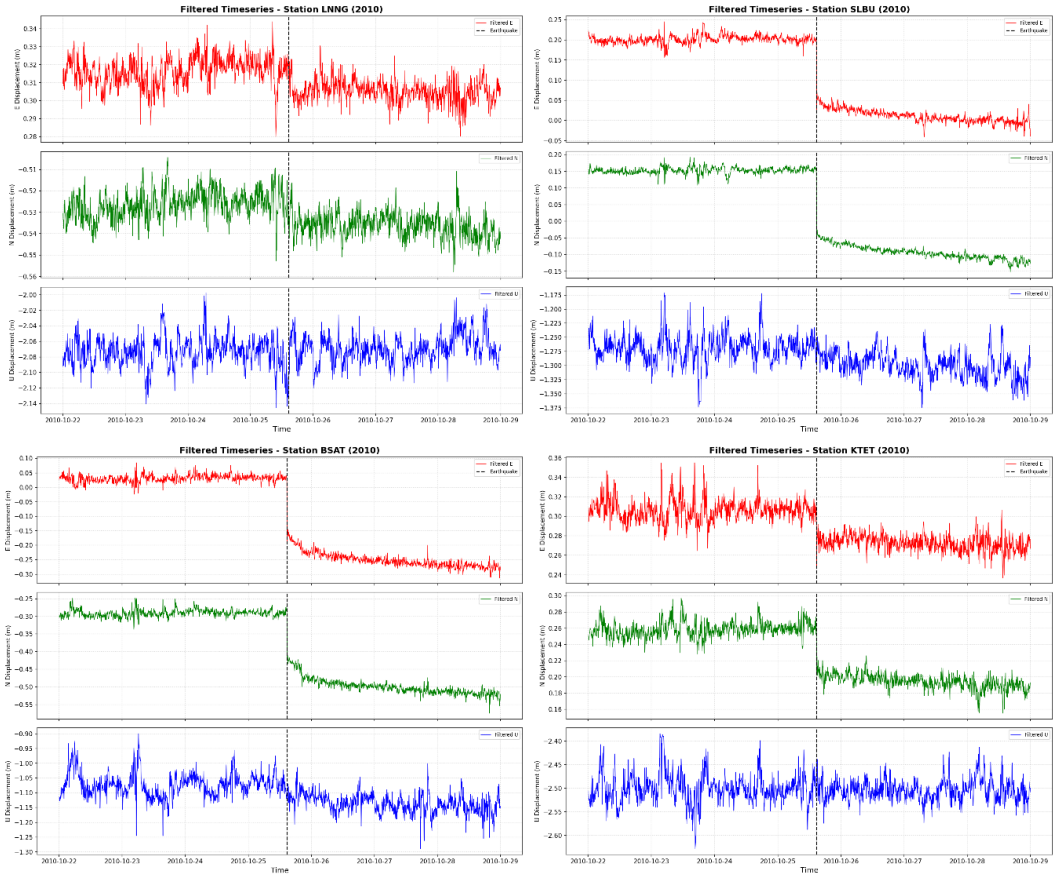

Fig. 3 *Time series of kinematic displacement for the vertical, east, and north components for particular near-field locations (e.g., SLBU, BSAT, KTET, LNNG). The red,green,blue scatter points represent 15-second kinematic east, north, uplift position estimates. capturing the instantaneous coseismic offset at t=0 and the subsequent rapid postseismic decay. Note the distinct 4–6 cm subsidence (downward shift) in the vertical component, confirming the offshore nature of the rupture.*

The coseismic rupture is indicated by a dramatic, immediate offset that occurs precisely at the moment of the earthquake, as shown by the horizontal components of the time series. This is immediately followed by a rapid, non-linear transient motion that continues in the same direction but decays in velocity over time. For example, the East component at station SLBU shows a sudden jump followed by a smooth logarithmic curve that persists for days. This ability to track the post-rupture motion second-by-second allows us to separate the true coseismic step from the

subsequent rapid afterslip, a distinction that is often blurred in conventional daily processing where the first 24 hours of motion are averaged into a single data point.

Crucially, the vertical (normal) time series at the Pagai Island stations provide a definitive geometric constraint on the rupture source. As illustrated in the vertical component plots in Fig. 3, stations SLBU and BSAT reveal an instantaneous and stable subsidence, or downward displacement, of approximately 4 to 6 cm. This vertical signal is stable throughout the postseismic phase and is a critical piece of evidence regarding the earthquake's mechanism. The location of the station in relation to the slip patch determines whether the ground moves upward or downward in the context of subduction zone seismicity.

Surface subsidence at the location of the Pagai Islands confirms that the primary slip patch was located offshore, well to the southwest of the islands. If the rupture had extended downdip beneath the islands, geodetic theory predicts that we would have observed surface uplift. Therefore, the widespread subsidence recorded in the kinematic time series provides strong, independent evidence that the 2010 event was a "tsunami earthquake," characterized by a rupture confined to the shallow, compliant sedimentary wedge near the trench, rather than a deep megathrust event.

3.2 Coseismic Displacement Field and Rupture Characteristics

The coseismic offsets extracted from the kinematic time series exhibit a coherent spatial pattern consistent with a shallow subduction rupture. The stations on the North and South Pagai Islands, which are situated precisely above the downdip border of the rupture patch, recorded the greatest displacements, as shown in Fig. 4. The vector map indicates that the main motion occurred in the direction of the trench, southwest. Specifically, stations SLBU and BSAT experienced horizontal trench-ward motions ranging from 20 to 25 cm. These values are substantial but relatively moderate for a magnitude 7.8 event, further suggesting that the main energy release was distant from the islands.

The quantitative values for these offsets are detailed in Table 3. For instance, station BSAT recorded a coseismic eastward displacement of -25.43 cm and a northward displacement of -18.31 cm. Similarly, in the East and North components, station PRKB recorded -13.87 cm and -9.59 cm, respectively. These precise static offsets serve as the input for any finite fault inversion and define the starting point for the postseismic relaxation analysis. By using kinematic estimation, we ensure that these values reflect the true elastic rebound at the moment of the quake, uncontaminated by the rapid afterslip that occurred in the subsequent hours.

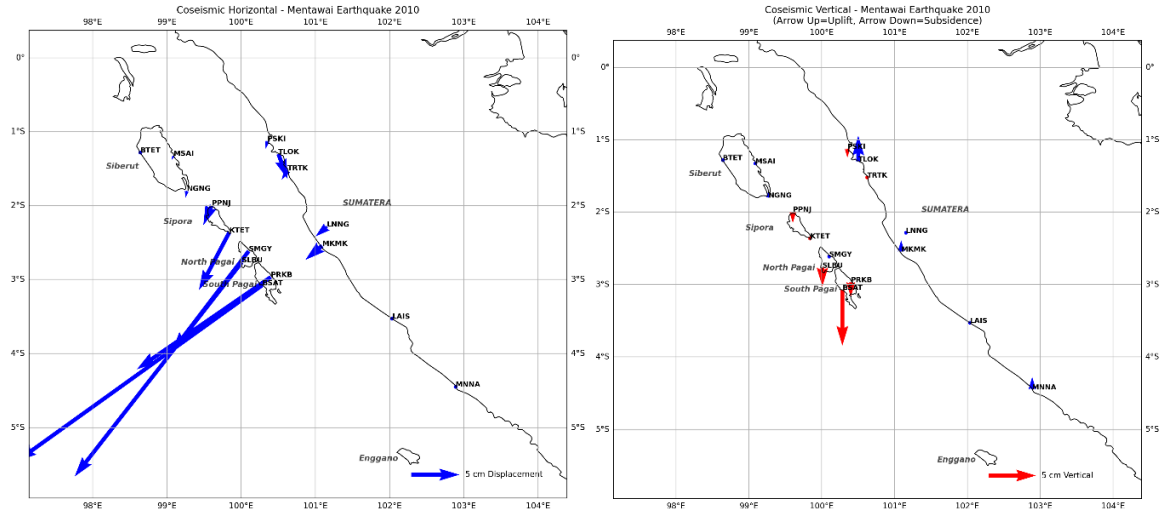

Fig. 4 *Horizontal (left) and vertical (right) coseismic displacement fields of the 2010 Mw 7.8 Mentawai earthquake derived from sub-daily kinematic PPP solutions. The vectors indicate moderate trench-ward motion and subsidence at the Pagai islands, consistent with a shallow offshore rupture.*

The vertical displacement field, also shown in Fig. 4 (right Fig.), reinforces the interpretation of a shallow source. The widespread subsidence of 4 to 6 cm across the Pagai Islands is consistent across multiple stations, ruling out local site effects. This pattern of moderate horizontal motion coupled with consistent subsidence is the geodetic fingerprint of a shallow rupture that did not propagate significantly downdip. It suggests that the slip was focused in the megathrust's updip section, where the contact usually displays frictional behavior that weakens with velocity.

Furthermore, the deformation field displays a rapid spatial decay in magnitude with distance from the trench. Stations located farther inland on the island of Sipora (e.g., KTET) and on the Sumatran mainland register progressively smaller displacements. For example, station KTET recorded only about 3 cm of horizontal motion, and mainland stations showed negligible offsets. Unlike conventional megathrust ruptures that cause extensive deformation along the whole forearc and mainland, this strong localization of deformation in the outer forearc wedge demonstrates that the 2010 Mentawai earthquake was a highly localized shallow event.

3.3 Early Postseismic Deformation and Decay Analysis

Following the instantaneous coseismic step, the kinematic solutions reveal that the crust did not immediately reach equilibrium but instead underwent a significant and rapid transient deformation phase. Fig. 5 (top Fig.) visualizes the cumulative postseismic displacement vectors over increasing time intervals, from the first 30 minutes up to 3 days. Spatially, the postseismic motion generally aligns with the azimuth of the coseismic slip but demonstrates a distinct spatial extension. The vectors at the Pagai Islands point trench-ward, but their significant magnitude suggests that the deformation zone migrated downdip from the coseismic rupture patch into the deeper plate interface beneath the islands.

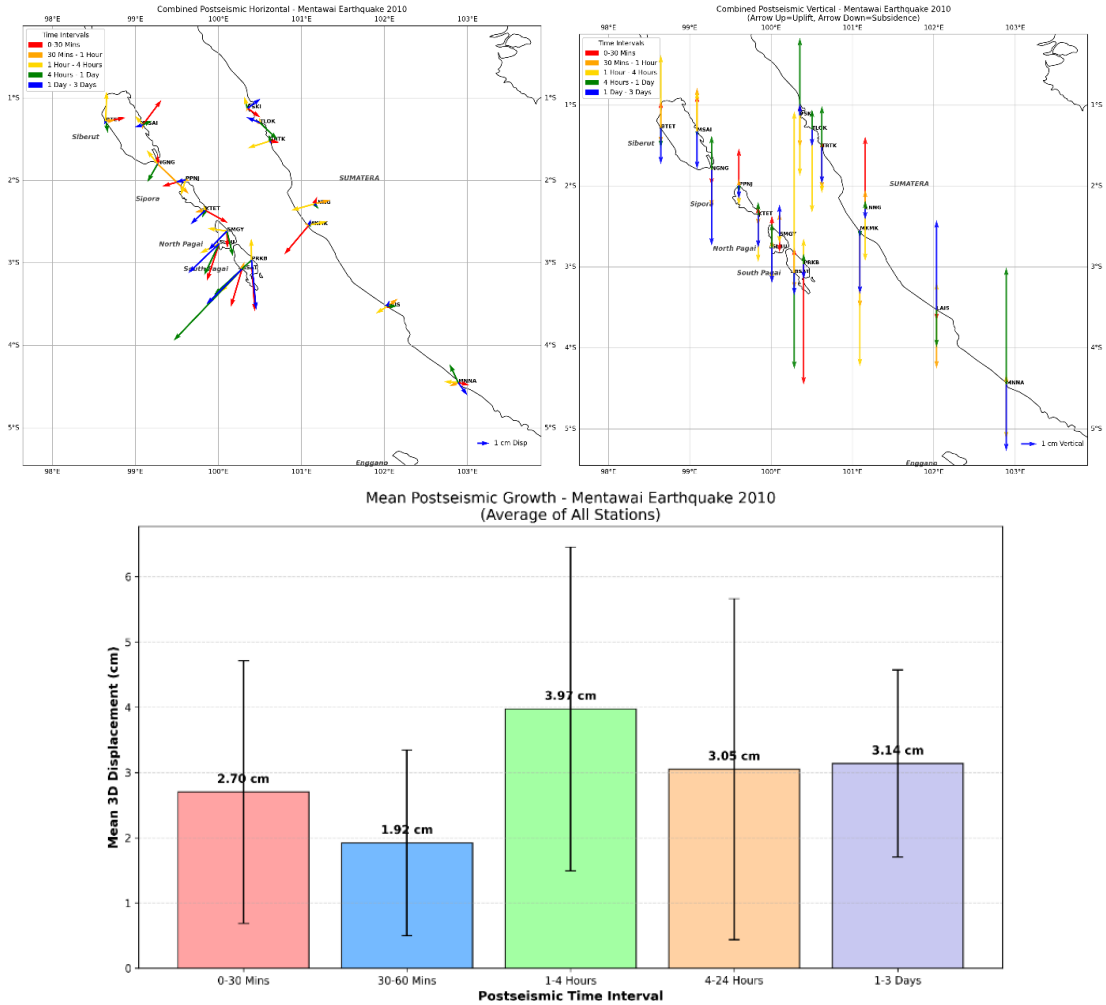

Fig. 5 *Spatiotemporal evolution of early postseismic deformation. (Top) Cumulative postseismic displacement vectors over varying time intervals. (Bottom) Mean 3D cumulative displacement growth across all stations, highlighting the rapid accumulation within the first 4 hours.*

The rapidity of this early postseismic phase is quantitatively analyzed in the mean 3D displacement growth chart shown in Fig. 5 (bottom Fig.). This analysis reveals that a substantial portion of the total afterslip occurred almost immediately. On average, a displacement of 2.70 cm was accumulated within the first 30 minutes post-rupture. This was followed by an additional 1.92 cm in the subsequent 30-minute interval and a massive 3.97 cm over the next 1–4 hours. This means that the fault continued to slide rapidly even after the seismic waves had subsided, releasing a significant amount of stored strain energy in the form of aseismic creep.

Comparing these intervals reveals the critical importance of sub-daily observation. The displacement accumulated in the first 4 hours alone (approximately 8.6 cm cumulative) is significantly larger than the total displacement observed over the entire subsequent 1–3 day period, which amounted to only 3.14 cm. This finding indicates that the decay of afterslip velocity is extremely steep; the fault moves fastest immediately after the break. If one were to rely solely on daily GPS solutions, this entire 4-hour period of rapid motion would be averaged out, leading to a severe underestimation of the initial postseismic velocity.

This spatiotemporal evolution suggests a mechanical continuity between the seismic rupture and the aseismic afterslip. The stress released by the shallow rupture was transferred to the adjacent downdip segment of the fault. Because this deeper segment has different frictional properties specifically, it is velocity-strengthening it did not rupture seismically but instead responded by sliding stably at a high rate. The border between the locked zone that broke and the creeping zone that slid silently is successfully mapped by the kinematic data.

3.4 Decay Mechanism and Physical Interpretation

To understand the physical process driving this rapid transient motion, we modeled the displacement time series using two competing decay functions: logarithmic (Eq. 1) and exponential (Eq. 2). Determining which mathematical model best fits the data is essential because different models correspond to different rheological mechanisms. Logarithmic decay is typically associated with frictional afterslip on a fault interface, whereas exponential decay is indicative of linear viscoelastic relaxation of the mantle. We fitted both models to the 15-second kinematic position estimates for all near-field stations.

Table 1 *Estimated parameters and RMS misfits for the Logarithmic decay model.*

Site	Logarithmic				RMS
	a_{East} (cm)	a_{North} (cm)	C_{east} (cm)	C_{north} (cm)	
BSAT	-2.995	-2.683	-17.134	-42.782	0.841
BTET	-0.065	-0.023	-3.203	-66.888	0.518
KTET	-0.267	-0.631	27.987	21.125	0.728
LAIS	-0.203	-0.056	17.8	-19.301	0.631
LNNG	-0.18	-0.107	30.974	-53.291	0.529
MKMK	-0.102	-0.034	18.9	-51.398	0.552
MNNA	-0.101	-0.168	12.407	4.478	0.742
MSAI	-0.049	-0.124	30.241	6.335	0.682
NGNG	0.031	-0.312	42.22	5.756	1.112
PPNJ	-0.07	-0.124	29.418	-60.657	0.59
PRKB	-1.488	-1.075	23.935	-42.469	1.292
PSKI	-0.065	0.018	8.198	-33.397	0.607
SLBU	-1.711	-2.288	5.688	-3.181	0.622
SMGY	-0.709	-0.957	32.508	16.302	0.753
TLOK	-0.863	0.301	134.662	-196.4	2.177
TRTK	-0.064	-0.153	5.337	-72.901	0.452

The statistical results, summarized in Table 1 and Table 2, unequivocally favor the logarithmic model. We used the Root Mean Square (RMS) misfit to evaluate the goodness-of-fit. For example, at station BSAT, the exponential model yields an RMS misfit of 0.926 cm, but the logarithmic model achieves an RMS misfit of 0.841 cm. A similar pattern is observed at station PRKB, where the logarithmic fit (RMS 1.292 cm) consistently outperforms the exponential fit (RMS 1.300 cm). Across the entire network, the logarithmic function provides a closer approximation to the observed data, minimizing the residuals between the modeled curve and the actual GPS observations.

Table 2 *Estimated parameters and RMS misfits for the Exponential decay model.*

Site	Exponential				RMS
	a_{East} (cm)	a_{North} (cm)	C_{east} (cm)	C_{north} (cm)	
BSAT	-8.774	-7.808	-18.805	-44.313	0.926
BTET	-0.208	-0.047	-3.227	-66.914	0.518
KTET	-0.81	-1.872	27.858	20.788	0.728
LAIS	-0.654	-0.141	17.729	-19.349	0.631
LNNG	-0.534	-0.281	30.877	-53.373	0.53
MKMK	-0.342	-0.122	18.873	-51.401	0.551
MNNA	-0.314	-0.499	12.362	4.388	0.742
MSAI	-0.168	-0.358	30.23	6.263	0.683
NGNG	0.095	-0.979	42.235	5.625	1.109
PPNJ	-0.23	-0.364	29.395	-60.726	0.59
PRKB	-4.312	-3.136	23.072	-43.079	1.3
PSKI	-0.211	0.054	8.177	-33.387	0.607
SLBU	-5.088	-6.776	4.787	-4.408	0.632
SMGY	-2.09	-2.833	32.121	15.789	0.755
TLOK	-2.956	1.054	134.46	-196.344	2.173
TRTK	-0.191	-0.426	5.305	-73	0.453

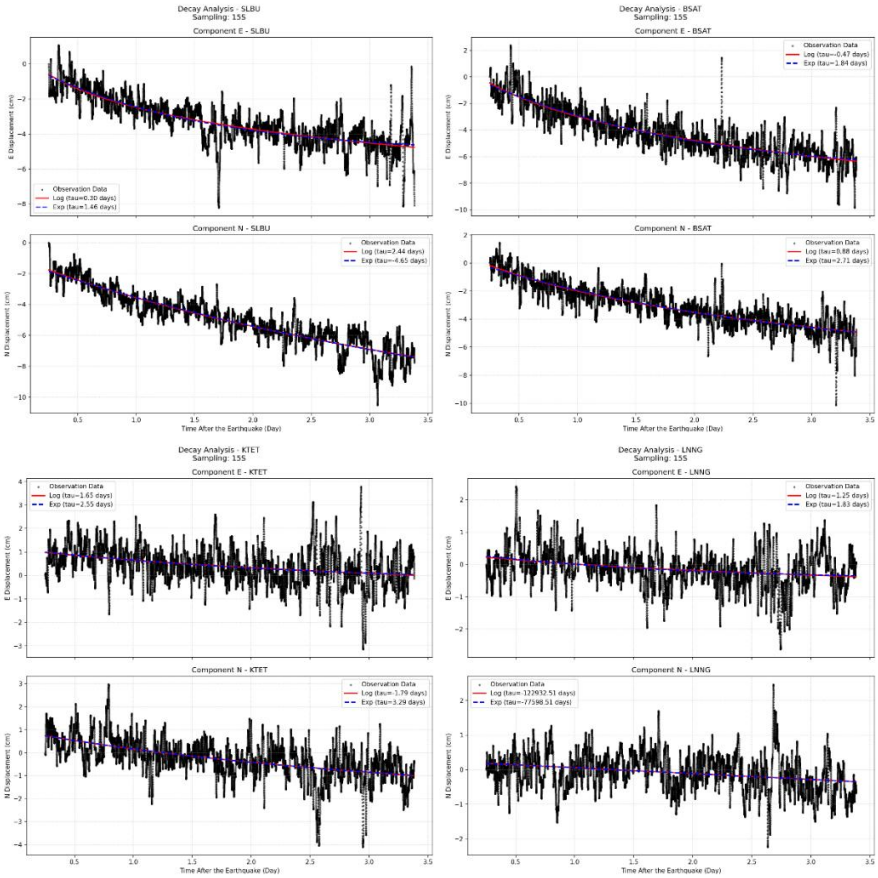

Fig. 6 *Kinematic displacement time series (black/grey dots) for North and East components. The best-fit logarithmic model is shown by red line, and the exponential model is shown by blue line. Note how the red line better fits the rapid initial motion.*

Visually, this preference is evident in Fig. 6, where the best-fit curves are overlaid on the kinematic time series. The logarithmic curve (indicated by the solid red line) tracks the dense cloud of data points with high fidelity,

particularly during the critical first 24 hours where the curvature of the displacement signal is sharpest. In contrast, the exponential curve (indicated by the blue dashed line) often fails to reproduce this rapid onset, tending to underestimate the initial velocity and overestimate the later deformation. The visual mismatch of the exponential model confirms that viscoelastic processes are too slow to explain the immediate post-earthquake deformation.

The parameters derived from the logarithmic modeling further support the afterslip hypothesis. As detailed in Table 1, the estimated characteristic decay times (τ) are extremely short, ranging from approximately 0.05 to 0.3 days. For example, the East component at station SLBU exhibits a decay time of roughly 0.30 days. This extremely short timescale is a hallmark of rate-and-state friction mechanics, where the fault response to a stress step is immediate and decays inversely with time. Therefore, we conclude that frictional afterslip on the megathrust interface specifically in the velocity-strengthening zone downdip of the rupture was the dominant driver of deformation in the days following the 2010 Mentawai earthquake.

3.5 Comparison of Coseismic and Postseismic Budgets

A direct comparison of the coseismic offsets and the cumulative early postseismic displacements highlights the significant contribution of afterslip to the total deformation budget. By integrating the postseismic motion over a 3-day interval, we can assess how much additional slip occurred relative to the mainshock. The comparative values for all stations are summarized in Table 3. While the coseismic slip dominates the overall magnitude of displacement, the early afterslip contributes a remarkably large fraction, ranging from 10% to 40% of the total surface displacement at near-field stations.

The most significant postseismic contributions are observed at stations located closest to the downdip edge of the rupture. For example, Table 3 shows that station BSAT recorded a massive postseismic displacement of -11.77 cm in the East component and -11.34 cm in the North component. When compared to its coseismic offset of -25.43 cm (East) and -18.31 cm (North), the afterslip represents a substantial continuation of the fault motion. Similarly, station SLBU recorded a postseismic northward motion of -9.41 cm, which corresponds to approximately 42% of its coseismic jump (-22.24 cm). These high ratios indicate that the earthquake was not a singular event but rather the beginning of a prolonged slip episode.

Table 3 *Comparison of Coseismic offsets versus cumulative Early Postseismic displacements.*

Site	Coseismic		Postseismic	
	E (cm)	N (cm)	E (cm)	N (cm)
BSAT	-25.43	-18.31	-11.77	-11.34
BTET	0.1	0.07	-0.58	0.76
KTET	-3.14	-5.98	-0.64	-3.51
LAIS	-0.02	-0.2	-0.57	-0.52
LNNG	-1.18	-1.01	-1.15	-0.76
MKMK	-1.74	-1.47	-1.07	-1.81
MNNA	0.07	0.23	0.43	0.25
MSAI	-0.19	-0.42	-1.03	1.05
NGNG	-0.12	-0.71	0.02	-0.63
PPNJ	-0.86	-2.07	0.03	-0.66
PRKB	-13.87	-9.59	-4.94	-7.36
PSKI	-0.17	-0.8	-0.03	0.24
SLBU	-17.28	-22.24	-6.49	-9.41
SMGY	-7.93	-10.43	-2.39	-4.48
TLOK	0.96	-2.6	-0.59	-0.76
TRTK	-0.6	-0.99	0.24	-1.73

The spatial distribution of these high-amplitude postseismic signals is visualized in Fig. 7. The comparison map shows that while the black coseismic vectors are large, the red postseismic vectors are far from negligible, particularly at the Pagai Islands. This implies that creeping patches downdip of the main slip zone were instantly activated by the stress changes brought on by the shallow seismic rupture. This downdip region's high afterslip magnitude suggests that a sizable amount of the plate convergence budget is released aseismically.

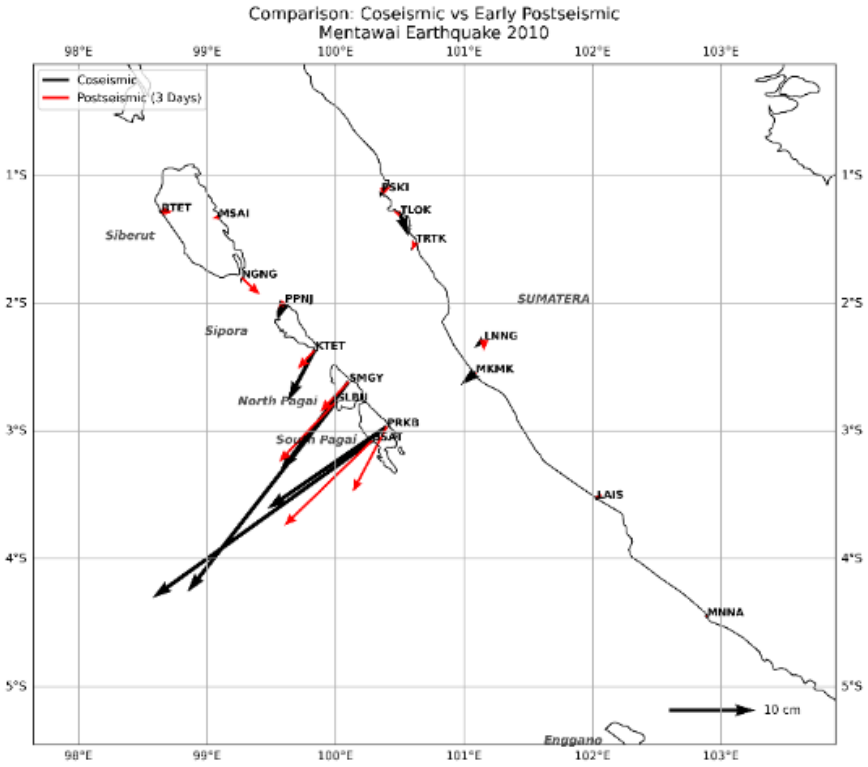

Fig. 7 *Comparison of coseismic (black vectors) and early postseismic (red vectors) displacement fields.*

Conversely, far-field stations such as LAIS and MKMK exhibit minimal postseismic influence, with displacements generally less than 1 cm. This sharp contrast confirms that the rapid afterslip observed in this study is a near-field phenomenon, confined to the segment of the megathrust immediately adjacent to the rupture. These results paint a picture of a heterogeneous frictional landscape along the Mentawai segment, characterized by a sharp transition from a shallow velocity-weakening zone that ruptures in tsunamigenic earthquakes to a deeper velocity-strengthening zone that creeps silently in their aftermath.

4 Conclusion

This study utilized high-rate kinematic GPS observations to characterize the deformation field of the 2010 Mw 7.8 Mentawai tsunami earthquake, effectively resolving both the instantaneous rupture and the rapid afterslip phase. The primary results are:

- The coseismic displacement field shows up to 20–25 cm of horizontal motion and 4–6 cm of vertical subsidence, confirming a very shallow rupture concentrated near the trench.
- Early postseismic deformation, typically obscured in daily GPS solutions, was clearly detected and spans the first minutes to days after the earthquake. These signals reach several centimeters in amplitude and evolve smoothly.
- Logarithmic decay models fit the postseismic trajectories better than exponential models, indicating that frictional afterslip dominates the early deformation phase. Characteristic decay times are on the order of a few days.
- The spatial pattern suggests that afterslip occurred downdip of the main rupture, highlighting a strongly heterogeneous fault interface where seismic rupture in the shallow prism transitions rapidly to aseismic slip at depth.

These insights significantly advance our knowledge regarding the mechanics of tsunami earthquakes and clarify the complex interaction between seismic rupture and aseismic creep along the Sunda subduction zone.

Acknowledgement

We extend our sincere gratitude to Institut Teknologi Sepuluh Nopember (ITS) for funding this work under the research grant titled "Spatiotemporal Variations of Coseismic and Early Afterslip Deformation of >M7 Earthquakes Along the Sumatra-Java Subduction Zone Using Kinematic GNSS." This financial assistance was pivotal in ensuring the successful execution and publication of this research.

References

1. K. Sieh, "The Sunda megathrust - Past, present and future," Journal of Earthquake and Tsunami, vol. 1, no. 01, pp. 1–19, 2007.
2. A. V. Newman, G. Hayes, Y. Wei, and J. Convers, "The 25 October 2010 Mentawai tsunami earthquake, from real-time discriminants, finite-fault rupture, and tsunami excitation," Geophysical Research Letters, vol. 38, no. 5, 2011.
3. E. M. Hill et al., "The 2010 Mw 7.8 Mentawai earthquake: Very shallow source of a rare tsunami earthquake determined from tsunami field survey and near-field GPS data," Journal of Geophysical Research: Solid Earth, vol. 117, no. B6, 2012.
4. R. Cattin et al., "Stress change and effective friction coefficient along the Sumatra-Andaman-Sagaing fault system after the 26 December 2004 (Mw = 9.2) and the 28 March 2005 (Mw = 8.7) earthquakes," Geochemistry, Geophysics, Geosystems, vol. 10, no. 3, 2009.
5. C. J. Marone, C. H. Scholz, and R. Bilham, "On the mechanics of earthquake afterslip," Journal of Geophysical Research: Solid Earth, vol. 96, no. B5, pp. 8441–8452, 1991.
6. H. Perfettini et al., "Seismic and aseismic slip on the central Peru megathrust," Nature, vol. 465, no. 7294, pp. 78–81, 2010.
7. L. L. H. Tsang et al., "Afterslip following the 2007 Mw 8.4 Bengkulu earthquake in Sumatra loaded the 2010 Mw 7.8 Mentawai tsunami earthquake rupture zone," Journal of Geophysical Research: Solid Earth, vol. 121, pp. 9034–9049, 2016.
8. K. Liu et al., "Rapid early afterslip characteristics of the 2010 moment magnitude (Mw) 8.8 Maule earthquake determined with sub-daily GPS solutions," Satellite Navigation, vol. 5, no. 23, 2024.
9. C. Twardzik, M. Vergnolle, A. Sladen, and A. Avallone, "Unravelling the contribution of early postseismic deformation using sub-daily GNSS positioning," Scientific Reports, vol. 9, p. 1775, 2019.
10. Y. Bock and D. Melgar, "Physical applications of GPS geodesy: A review," Reports on Progress in Physics, vol. 79, no. 10, 2016.
11. M. Chlieh et al., "Heterogeneous coupling of the Sumatran megathrust constrained by geodetic and paleogeodetic measurements," Journal of Geophysical Research: Solid Earth, vol. 113, no. B5, 2008.
12. A. P. Kositsky and J.-P. Avouac, "Inverting geodetic time series with a principal component analysis-based inversion method," Journal of Geophysical Research: Solid Earth, vol. 115, no. B3, 2010.
13. R. Raharja et al., "Long aseismic slip duration of the 2006 Java tsunami earthquake based on GPS data," Earthquake Science, vol. 29, no. 5, pp. 291–298, 2016.
14. W. Bertiger et al., "GipsyX/RTGx: A new tool for geodetic analysis," GPS Solutions, vol. 24, no. 4, 2020.
15. J. F. Zumberge, M. B. Heflin, D. C. Jefferson, M. M. Watkins, and F. H. Webb, "Precise point positioning for the efficient and robust analysis of GPS data from permanent stations," Journal of Geophysical Research: Solid Earth, vol. 102, no. B3, pp. 5005–5017, 1997.